# Exceptional Points of Degeneracy Directly Induced by Space–Time Modulation of a Single Transmission Line

Kasra Rouhi, Hamidreza Kazemi, Alexander Figotin, and Filippo Capolino, Fellow, IEEE

Abstract—We demonstrate how exceptional points of degeneracy (EPDs) are induced in a single transmission line (TL) directly by applying periodic space-time modulation to the per-unit-length distributed capacitance. In such space-time modulated (STM) TL, two eigenmodes coalesce into a single degenerate one, in their eigenvalues (wavenumbers), and eigenvectors (voltage-current states) when the system approaches the EPD condition. The EPD condition is achieved by tuning a parameter in the space-time modulation, such as spatial or temporal modulation frequency, or the modulation depth. We unequivocally demonstrate the occurrence of the EPD by showing that the bifurcation of the wavenumber around the EPD is described by the Puiseux fractional power series expansion. We show that the first-order expansion is sufficient to approximate well the dispersion diagram, and how this "exceptional" sensitivity of the STM-TL's wavenumber to tiny changes of any TL or modulation parameter enables a possible application as a highly sensitive TL sensor when operating at an EPD.

*Index Terms*—Exceptional point of degeneracy (EPD), perturbation theory, sensor, space–time modulation, transmission lines (TLs).

# I. INTRODUCTION

RECENT advancements in exceptional point of degeneracy (EPD) concepts have attracted a surge of interests due to their potential benefits in various electromagnetic applications. An EPD is a point in the parameter space of a system at which multiple eigenmodes coalesce in both their eigenvalues and eigenvectors. The concept of EPD has been studied in lossless, spatially [1]–[3] or temporally [4], [5] periodic structures, and in systems with loss and/or gain under parity-time symmetry [6]–[9]. Since the characterizing feature of an exceptional point is the strong full degeneracy of at least two eigenmodes, as implied in [10], we stress the importance of referring to it as a "degeneracy" and, hence, of including the D in EPD. In essence, an EPD is obtained when the system matrix is similar to a matrix that comprises a nontrivial Jordan block [1], [11]–[13]; here,

Manuscript received April 22, 2020; revised July 8, 2020; accepted July 17, 2020. Date of publication August 4, 2020; date of current version November 23, 2020. This work was supported by the National Science Foundation under Grant ECCS-1711975. (Corresponding author: Filippo Capolino.)

Kasra Rouhi, Hamidreza Kazemi, and Filippo Capolino are with the Department of Electrical Engineering and Computer Science, University of California, Irvine, CA 92697 USA (e-mail: kasra.rouhi@uci.edu; hkazemiv@uci.edu; f.capolino@uci.edu).

Alexander Figotin is with the Department of Mathematics, University of California, Irvine, CA 92697 USA (e-mail: afigotin@uci.edu).

Digital Object Identifier 10.1109/LAWP.2020.3014112

however, the formulation leads to a matrix of infinite dimensions, and therefore we assess the occurrence of the EPD by invoking the Puiseux fractional power expansion series [14] to describe the bifurcation of the dispersion diagram at the EPD. There are several features associated with the development of EPDs, which lead to applications, such as active systems gain enhancement in waveguides [15]–[17], and enhanced sensing [18]–[21].

Researchers have been studying how to incorporate time variation of parameters into electromagnetic systems with the goal of adding new degrees of freedom in wave manipulation. In their pioneering work, Cassedy and Oliner [22], [23] studied the dispersion characteristics of wave propagation in a medium with dielectric constant modulated as a traveling-wave with sinusoidal form. Then, Elachi [24] studied electromagnetic wave propagation and the wave vector diagram in general space-time periodic materials for different wave polarization. In [25] and [26], the authors analyzed the concept of temporal photonic crystals with periodic modulation of permeability and permittivity. In [27], magnetless nonreciprocity was demonstrated in spatiotemporally modulated coupled-resonator networks. Also, Taravati and Caloz [28] proposed a mixer-duplexer-antenna leakywave system based on periodic space-time modulation. Recently, in [29], space–time modulation was employed to control phase and amplitude tunability in a metasurface. Several other papers have been published on time/space-time modulation to generate nonreciprocity in electromagnetic structures [30]–[33]. In all these works, the concept of EPD in such modulated structures was not studied.

Here we leverage on the two concepts of space–time modulation and EPD and develop a general scheme to realize EPDs in space–time periodic single transmission line (TL) that could be used as a sensor. We investigate the occurrence of EPDs when the per-unit-length capacitance is modulated in space and time, by showing that the bifurcation of the dispersion diagram around the EPD is well approximated by the Puiseux fractional power series expansion. This EPD-related fractional expansion is also used to explain the extreme sensitivity of the wavenumber to perturbation of system parameters adding a degree of freedom to TL systems with space-only or time-only modulation.

### II. DEGENERACIES IN A UNIFORM SINGLE STM-TL

Degeneracies in wave propagation in an infinitely long TL is examined when the per-unit-length capacitance is modulated in

1536-1225 © 2020 IEEE. Personal use is permitted, but republication/redistribution requires IEEE permission. See https://www.ieee.org/publications/rights/index.html for more information.

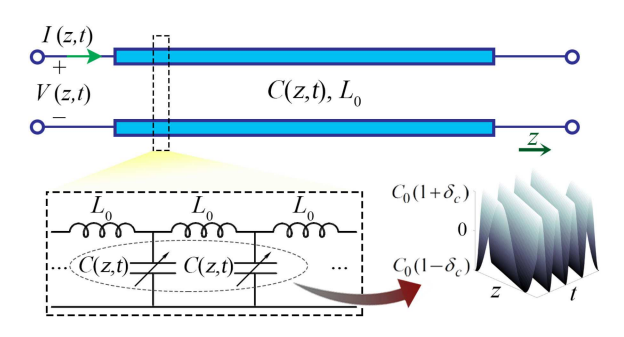


Fig. 1. Schematic illustration of a single TL with space–time modulation of the distributed capacitance. We also show the equivalent TL circuit with the per-unit-length inductor and modulated capacitor.

both space and time. We employ the formalism and description of a linear TL shown in [34]. A schematic representation of a space—time modulated (STM) TL is shown in Fig. 1, where only the per-unit-length capacitance is space—time varying, while the per-unit-length inductance is constant throughout the TL. Without loss of generality, we assume sinusoidal space—time variation; however, EPDs can be induced also by other forms of periodic space—time variation. The distributed per-unit-length space—time varying capacitance is given by

$$C(z,t) = C_0 + C_m(t) = C_0(1 + \delta_c \cos(\omega_m t - \beta_m z))$$
 (1)

where  $C_0$  is the space–time averaged (i.e., unmodulated) perunit-length capacitance,  $\delta_c$  is the modulation depth, and  $\omega_m$  and  $\beta_m$  are the temporal and spatial modulation frequencies, respectively. The dynamic behavior of such a TL is captured by using the Telegrapher's equations, which are represented in terms of a voltage and current state vector,  $\Psi(z,t) = [V(z,t), I(z,t)]^T$ , where the superscript T denotes the transpose operation. The dynamic behavior of this state vector is described by the first-order differential equations given as

$$\partial_{\mathbf{z}} \Psi(z,t) = -\partial_{\mathbf{t}} \left( \underline{\mathbf{M}}(z,t) \Psi(z,t) \right) \tag{2}$$

where the STM  $2 \times 2$  system matrix  $\underline{\mathbf{M}}$  is given by

$$\underline{\underline{\mathbf{M}}}(z,t) = \begin{bmatrix} 0 & L_0 \\ C(z,t) & 0 \end{bmatrix} . \tag{3}$$

We look for time-harmonic solutions, and because of the periodic nature of the modulation, the state vector eigensolution is cast into an infinite space-time Floquet-Bloch series as

$$\Psi(z,t) = e^{j(\omega t - \beta z)} \sum_{q = -\infty}^{\infty} \Psi_q \, e^{jq(\omega_{\rm m} t - \beta_{\rm m} z)} \tag{4}$$

where  $\beta$  and  $\omega$  are the propagation wavenumber and the angular frequency, respectively, and  $\Psi_q = [V_q,\ I_q]^{\rm T}$  is the complex amplitude of the qth harmonic of the state vector. We expand the space—time varying distributed capacitance in (1) in terms of its Fourier series

$$C(z,t) = \sum_{s=-1}^{1} C_s e^{js(\omega_{\rm m}t - \beta_{\rm m}z)}$$

$$\tag{5}$$

where  $C_s$  represents the amplitude of the sth harmonic. Substituting (4) and (5) in (2) and taking the time and space derivatives, the equation for each qth harmonic's  $\Psi_q$  is obtained as

$$\sum_{q=-\infty}^{\infty} (\beta + q\beta_{\rm m}) \Psi_q e^{jq(\omega_{\rm m}t - \beta_{\rm m}z)}$$

$$= \sum_{q=-\infty}^{\infty} \sum_{s=-1}^{1} \begin{bmatrix} 0 & (\omega + q\omega_{\rm m})L_0\delta_{s,0} \\ (\omega + (q+s)\omega_{\rm m})C_s \\ \Psi_q e^{j(q+s)(\omega_{\rm m}t - \beta_{\rm m}z)} & 0 \end{bmatrix}$$
(6)

where  $\delta_{s,0}$  is the Kronecker delta. Since the exponential functions  $e^{jq(\omega_{\rm m}t-\beta_{\rm m}z)}$  form a complete orthogonal set of functions, we balance the coefficient of the exponential with the same q index leading to

$$(\beta + q\beta_{\rm m})\mathbf{\Psi}_{q}$$

$$= \sum_{s=-1}^{1} \begin{bmatrix} 0 & (\omega + q\omega_{\rm m})L_{0}\delta_{s,0} \\ (\omega + q\omega_{\rm m})C_{s} & 0 \end{bmatrix} \mathbf{\Psi}_{q-s}. \quad (7)$$

Isolating the term with the wavenumber, the above equation is rearranged as

$$\beta \Psi_q = \sum_{s=-1}^{1} \underline{\underline{\mathbf{N}}}_{q,s} \Psi_{q-s} \tag{8}$$

where

$$\underline{\underline{\mathbf{N}}}_{q,s} = \begin{bmatrix} -q\beta_{\mathrm{m}}\delta_{s,0} & (\omega + q\omega_{\mathrm{m}})L_{0}\delta_{s,0} \\ (\omega + q\omega_{\mathrm{m}})C_{s} & -q\beta_{\mathrm{m}}\delta_{s,0} \end{bmatrix}. \tag{9}$$

The above equation can be cast in terms of a large block three-diagonal matrix  $\underline{\mathbf{T}}$  as

$$\underline{\mathbf{T}}\boldsymbol{\Psi} = \beta\boldsymbol{\Psi} \tag{10}$$

that can be used to determine the system eigenvalues  $\beta$  and eigenvectors  $\Psi = [\Psi_{-Q}, ..., \Psi_0, ..., \Psi_Q]^T$ . A finite number 2Q + 1 of harmonics is sufficient to determine the STM-TL wave characteristics and the occurrence of EPDs; hence, the dimension of the matrix T is  $2(2Q+1) \times 2(2Q+1)$ . The real and imaginary parts of the wavenumber in the  $\beta$ - $\omega$  dispersion diagram are plotted in Fig. 2(a) and (b), respectively, for the STM-TL with parameters as follows. As specified, we have considered the sinusoidal modulation given in (1) where the modulation parameters are  $\delta_c = 0.3$ ,  $\omega_m = 0.05\omega_0$ , and  $\beta_{\rm m}=0.8\beta_0$ , where  $\beta_0=\omega_0/c$  is the free -space propagation wavenumber at  $\omega_0/(2\pi) = 10^9 \,\mathrm{s}^{-1}$ . Moreover, the TL parameters are  $L_0=282\,\mathrm{nH/m}$  and  $C_0=113\,\mathrm{pF/m}$ . Note that the modulation frequency does not need to be comparable to the one of the radio frequency wave. We consider 2Q + 1 = 21harmonics to calculate the dispersion diagram (we checked that a larger number provides the same result), but we show only the first two harmonics, i.e., the real part of their wavenumbers and the relevant imaginary parts. It is observed from the dispersion diagram in Fig. 2(a) that for an STM-TL the band-gap locations form a tilted line, which indicates nonsymmetric dispersion  $(\omega(-\beta) \neq \omega(\beta))$  in such a structure, as already pointed out

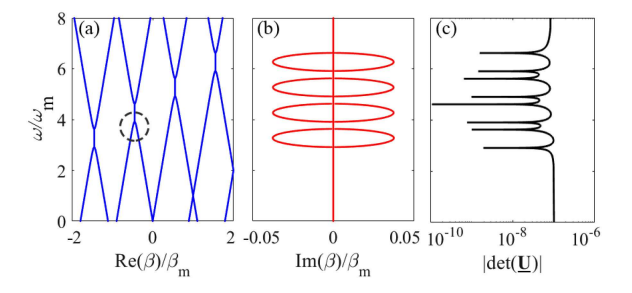


Fig. 2. Dispersion diagram of the STM-TL with second-order EPDs. (a) Real part of the wavenumber of first harmonics and (b) the corresponding imaginary parts, and (c) plot of  $|\det(\underline{\mathbf{U}})|$  versus frequency. The similarity transformation matrix  $\underline{\mathbf{U}}$  contains eigenvectors; therefore, the vanishing of  $|\det(\underline{\mathbf{U}})|$  is necessary at an EPD.

in [22] and [35]. Furthermore, it is clear from this figure that the eigenvalues, i.e., the propagation wavenumbers of the system, are coalescing at the band edges. To fully characterize an EPD, we have to show that the two eigenvectors corresponding to the two coalescing eigenvalues are also coalescing at the band edges. We define the similarity transformation matrix as  $\underline{\mathbf{U}} = [\mathbf{U}_1 \mid \cdots \mid \mathbf{U}_{2(2Q+1)}],$  where  $\underline{\mathbf{U}}_i$  is the eigenvector corresponding to the ith eigenvalue, and such matrix diagonalizes the system matrix as  $\mathbf{T} = \mathbf{U}\Lambda\mathbf{U}^{-1}$ . At the EPD, two eigenvectors become linearly dependent; therefore, we verify that  $|\det(\underline{\mathbf{U}})|$  vanishes at each EPD as a necessary condition, as shown in Fig. 2(c) [13]. Indeed, at  $\omega/\omega_{\rm m}=3.91$ , we observe that two eigenvalues as well as the two associated eigenvectors are equal to each other up to the six decimal digit. A sufficient condition to assess the occurrence of an EPD without looking directly at the eigenvectors is explained in the next section, by demonstrating that the dispersion diagram bifurcates at the EPD following the Puiseux fractional power expansion [14]. It is also possible to achieve EPDs in systems with space-only periodic modulation [13], [36], and such systems are reciprocal, or with time-only modulation [4]. space-time modulation adds a new degree of freedom to control the dispersion diagram's EPD position. Both temporal and spatial modulations are needed to obtain EPD at a desired frequency—wavenumber pair. This may be important to design highly tunable traveling-wave antennas since the radiation pointing angle and beamwidth depend on the wavenumber. From the dispersion diagram in Fig. 2(a), we observe that in an STM system, the band-gap locations form a tilted line; hence, the EPD positions in the dispersion diagram are nonreciprocal.

# III. PUISEUX FRACTIONAL POWER EXPANSION AND HIGH SENSITIVITY

Extreme sensitivity to system perturbations is an intrinsic characteristic of EPDs and this is intrinsically related to the Puiseux series [14], [37]–[39] that singularly describe the EPD occurrence. We first demonstrate how the dispersion diagram varies by changing different system parameters, then we show the extreme sensitivity of the wavenumber to a system perturbation when operating at an EPD that follows the description of the Puiseux fractional power expansion. We analyze the STM-TL wavenumbers by varying one system parameter at the time

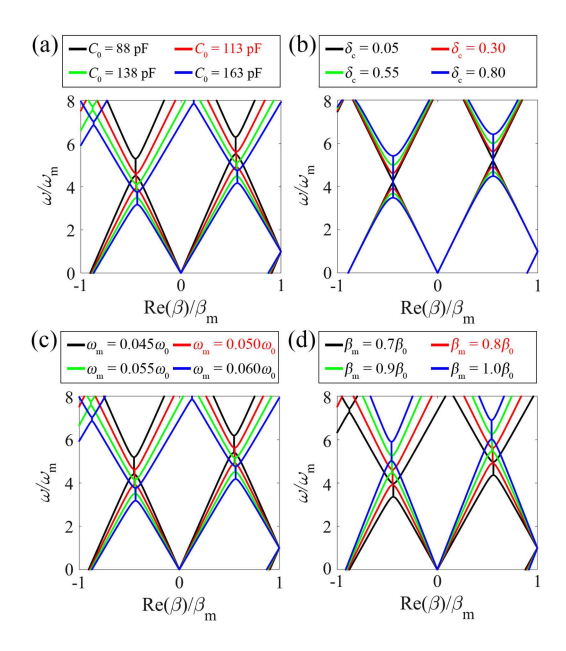


Fig. 3. Dispersion diagrams of the real part of wavenumbers by changing one single parameter at the time. The system parameters that are changed are (a)  $C_0$ , (b)  $\delta_{\rm c}$ , (c)  $\omega_{\rm m}$ , and (d)  $\beta_{\rm m}$ .

around the value used in the example. As a first parameter, we vary the unmodulated per-unit-length capacitance of the TL  $C_0$  and observe its effect on the dispersion diagram. As shown in Fig. 3(a), by increasing  $C_0$ , the dispersion diagram shifts downwards and consequently the EPDs move in the same direction. In the next step, we study the effect of the modulation depth  $\delta_c$  perturbation on the dispersion diagram in Fig. 3(b). By increasing the modulation depth, the band-gaps stretch out and become wider, meaning that EPDs at both edges of one band-gap move further apart from each other in frequency. As the third parameter, we explore the temporal modulation frequency  $\omega_{\rm m}$  variation on the location of the band-gaps and EPDs. Fig. 3(c) exhibits a similar trend of changes compared to those in Fig. 3(a). Finally, we examine the variation of spatial modulation frequency  $\beta_{\rm m}$  as shown in Fig. 3(d). It is seen from this figure that a different behavior is obtained compared to varying the previous parameters. Here, by increasing the spatial modulation frequency, band-gaps become wider and move toward higher frequency in the dispersion diagram; thus, EPDs move to higher frequencies as well. As a realistic scenario, we can utilize an STM-TL in high sensitivity applications. If an external substance or object is placed near the TL (for instance, the microstrip line), the TL's effective parameters would be perturbed, which in turn causes a large perturbation in the wavenumber that can be, in principle, easily detected.

As discussed in Section I, the eigenvalues at EPDs are exceedingly sensitive to perturbations of parameters of a time-varying system [4], [18], [20], [21]. Here we show that the sensitivity of a system's observable to a specific variation of a parameter is boosted due to the degeneracy of eigenmodes. As an example, we consider the first EPD in the first band-gap with the negative real part of wavenumber (indicated by a gray circle in Fig. 2) and we show how a modal wavenumber is perturbed by small system perturbations. We define the relative system perturbation

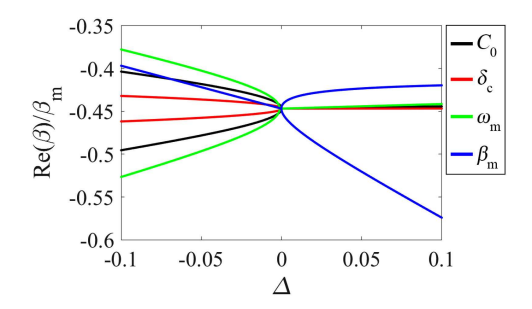


Fig. 4. Sensitivity of the real part of the propagation wavenumber to a parameter perturbation (one at the time) around the EPD.

 $\Delta$  as

$$\Delta = \frac{X_{\text{pert}} - X_{\text{EPD}}}{X_{\text{EPD}}} \tag{11}$$

where  $X_{\rm EPD}$  is the unperturbed parameter value that provides the EPD condition, and  $X_{\rm pert}$  is its perturbation. We consider variations of  $C_0$ ,  $\delta_{\rm c}$ ,  $\omega_{\rm m}$ , and  $\beta_{\rm m}$ , one at the time. The calculated real part of the wavenumber near the first EPD at  $\omega/\omega_{\rm m}=3.91$  is shown in Fig. 4. We conclude from the extracted results that the individual variation of the parameters of  $C_0$ ,  $\delta_{\rm c}$ , and  $\omega_{\rm m}$  shows similar sensitivity behavior, i.e., the real part of the wavenumber splits for  $\Delta<0$ . In contrast, variation of  $\beta_{\rm m}$  has an opposite effect on the dispersion diagram, i.e., the real part of the wavenumber splits for  $\Delta>0$ . Note that the  $\omega_{\rm m}$  perturbation shows the highest sensitivity. Higher sensitivity is obtained when the bifurcation of the dispersion diagram is wider. Furthermore, the  $\beta_{\rm m}$  perturbation response shows an opposite trend to that of the other three parameters.

We explain the extreme sensitivity by resorting to the general theory of EPDs. Note that a perturbation in  $\Delta$  value leads to a perturbed matrix  $\underline{\mathbf{T}}(\Delta)$ . Consequently, the two degenerate eigenvalues occurring at the EPD change considerably due to a small perturbation in  $\Delta$ , resulting in two distinct eigenvalues  $\beta_p(\Delta)$ , with p=1,2, close to the first EPD. The two perturbed eigenvalues near an EPD are represented by a single convergent Puiseux series (also called fractional power expansion) where the coefficients are calculated using the explicit recursive formulas given in [38]. An approximation of  $\beta_p(\Delta)$  around a second-order EPD is given by

$$\beta_p(\Delta) \approx \beta_{\text{EPD}} + (-1)^p \alpha_1 \sqrt{\Delta}.$$
 (12)

Following [37]–[39], we calculate  $\alpha_1$  as

$$\alpha_1 = \sqrt{\left(-\frac{\frac{\partial H}{\partial \Delta}(\Delta, \beta)}{\frac{1}{2!}\frac{\partial^2 H}{\partial \beta^2}(\Delta, \beta)}\right)}$$
(13)

evaluated at the EPD, i.e., at  $\Delta=0$  and  $\beta=\beta_{\rm EPD}$ , where  $H(\Delta,\beta)=\det[\underline{\mathbf{T}}(\Delta)-\beta\underline{\mathbf{I}}].$  Equation (12) indicates that for a small perturbation  $\Delta\ll 1$ , the eigenvalues change dramatically from their original degenerate value due to the square root function. As an indicative example, we consider the single STM-TL with parameters as used in Fig. 2. In this example, we select the EPD indicated by the gray circle in Fig. 2(a) with  $\omega/\omega_{\rm m}=3.91,$  and  $\beta_{\rm EPD}=-7.49\,{\rm m}^{-1}$  as the unperturbed EPD operation point. In this example, the perturbation parameter

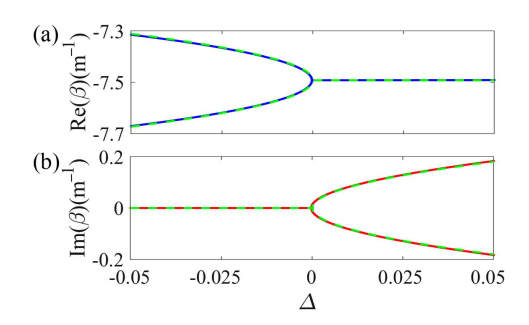


Fig. 5. Puiseux fractional power series expansion in (12) (green dashed lines) describes the bifurcation of the real and imaginary parts of the two wavenumbers when a system parameter ( $\delta_c$  in this case) is perturbed. The Puiseux series result is in excellent agreement with the wavenumbers evaluated using (10) (blue and red solid lines). (a) Real part. (b) Imaginary part.

is the modulation depth,  $\Delta = (\delta_c - \delta_{c,EPD})/\delta_{c,EPD}$ , and the Puiseux series coefficients are calculated as  $\alpha_1 = j0.81 \,\mathrm{m}^{-1}$ . The result in Fig. 5 exhibits the two branches of the exact perturbed eigenvalues  $\beta$  obtained from the eigenvalue problem in (10) when the system perturbation  $\Delta$  is applied. Moreover, this figure shows that such perturbed eigenvalues can be estimated with very good accuracy by employing the Puiseux series (green dashed lines) truncated at its first order. For a positive but small value of  $\Delta$ , the imaginary part of the eigenvalues experience a sharp change, while its real part remains constant. Moreover, a very small negative value of  $\Delta$  causes a rapid variation in the real part of the eigenvalues. This feature is actually one of the most extraordinary physical properties associated with the EPD concept, and it can be exploited for designing ultra-sensitive sensors [40], [41]. This kind of STM-TL with capacitance variation is feasible within the realm of current fabrication technologies. Varactor-loaded TL could be a proper alternative for implementing this kind of structure [42]. Recently, several tunable materials have been employed to conceive devices based on the spatiotemporal variation, such as graphene [43] and liquid crystal [44].

# IV. CONCLUSION

A single STM-TL supports EPDs of second order directly induced by spatiotemporal modulation of the distributed (perunit-length) capacitance. For its occurrence, an EPD does not need the presence of time-invariant gain or loss elements, as in PT symmetry, and it does not need two coupled TLs either. Here space and time modulations are not used to generate nonreciprocity or to enhance EPD properties but rather as a direct way to generate EPDs. This is in analogy to what was shown in [4] where time modulation was used to directly induce EPDs in a *single* resonator, without the need to resorting to two couple resonators with loss and gain as implied by PT symmetry [8]. We have investigated how to perturb an EPD condition by slightly perturbing system parameters and how this strongly modifies the degenerate eigenvector (i.e., the wavenumber). We have shown that small changes in a TL constitutive parameters lead to a very strong variation of the TL wavenumber and how this is predicted by the Puiseux fractional expansion series, suggesting a novel approach to design extremely sensitive sensors based on waveguide propagation.

## REFERENCES

- A. Figotin and I. Vitebskiy, "Oblique frozen modes in periodic layered media," *Phys. Rev. E*, vol. 68, no. 3, Sep. 2003, Art. no. 036609.
- [2] M. Y. Nada, M. A. K. Othman, and F. Capolino, "Theory of coupled resonator optical waveguides exhibiting high-order exceptional points of degeneracy," *Phys. Rev. B*, vol. 96, no. 18, Nov. 2017, Art. no. 184304.
- [3] M. A. K. Othman, F. Yazdi, A. Figotin, and F. Capolino, "Giant gain enhancement in photonic crystals with a degenerate band edge," *Phys. Rev. B*, vol. 93, no. 2, Jan. 2016, Art. no. 024301.
- [4] H. Kazemi, M. Y. Nada, T. Mealy, A. F. Abdelshafy, and F. Capolino, "Exceptional points of degeneracy induced by linear time-periodic variation," *Phys. Rev. Appl.*, vol. 11, no. 1, Jan. 2019, Art. no. 014007.
- [5] S. Longhi, "Floquet exceptional points and chirality in non-Hermitian Hamiltonians," J. Phys. A: Math. Theor., vol. 50, no. 50, Dec. 2017, Art. no. 505201.
- [6] C. M. Bender and S. Boettcher, "Real spectra in non-Hermitian Hamiltonians having PT symmetry," *Phys. Rev. Lett.*, vol. 80, no. 24, pp. 2455–2464, Jun. 1998.
- [7] W. D. Heiss, "Exceptional points of non-Hermitian operators," *J. Phys. A: Math. General*, vol. 37, no. 6, pp. 2455–2464, Jan. 2004.
- [8] J. Schindler, A. Li, M. C. Zheng, F. M. Ellis, and T. Kottos, "Experimental study of active LRC circuits with PT symmetries," *Phys. Rev. A*, vol. 84, no. 4, Oct. 2011, Art. no. 040101.
- [9] H. Hodaei, M.-A. Miri, M. Heinrich, D. N. Christodoulides, and M. Khajavikhan, "Parity-time symmetric microring lasers," *Science*, vol. 346, no. 6212, pp. 975–978, Nov. 2014.
- [10] M. V. Berry, "Physics of nonhermitian degeneracies," Czechoslovak J. Phys., vol. 54, no. 10, pp. 1039–1047, Oct. 2004.
- [11] A. Figotin and I. Vitebskiy, "Gigantic transmission band-edge resonance in periodic stacks of anisotropic layers," *Phys. Rev. E*, vol. 72, no. 3, Sep. 2005, Art. no. 036619.
- [12] M. A. K. Othman and F. Capolino, "Theory of exceptional points of degeneracy in uniform coupled waveguides and balance of gain and loss," *IEEE Trans. Antennas Propag.*, vol. 65, no. 10, pp. 5289–5302, Oct. 2017.
- [13] A. F. Abdelshafy, M. A. K. Othman, D. Oshmarin, A. T. Almutawa, and F. Capolino, "Exceptional points of degeneracy in periodic coupled waveguides and the interplay of gain and radiation loss: Theoretical and experimental demonstration," *IEEE Trans. Antennas Propag.*, vol. 67, no. 11, pp. 6909–6923, Nov. 2019.
- [14] T. Kato, Perturbation Theory for Linear Operators, vol. 132, 2nd ed. Berlin, Heidelberg: Springer-Verlag, 1995.
- [15] M. A. K. Othman, V. A. Tamma, and F. Capolino, "Theory and new amplification regime in periodic multimodal slow wave structures with degeneracy interacting with an electron beam," *IEEE Trans. Plasma Sci.*, vol. 44, no. 4, pp. 594–611, Apr. 2016.
- [16] A. F. Abdelshafy, M. A. K. Othman, F. Yazdi, M. Veysi, A. Figotin, and F. Capolino, "Electron-beam-driven devices with synchronous multiple degenerate eigenmodes," *IEEE Trans. Plasma Sci.*, vol. 46, no. 8, pp. 3126–3138, Aug. 2018.
- [17] M. Veysi, M. A. K. Othman, A. Figotin, and F. Capolino, "Degenerate band edge laser," *Phys. Rev. B*, vol. 97, no. 19, May 2018, Art. no. 195107.
- [18] J. Wiersig, "Sensors operating at exceptional points: General theory," *Phys. Rev. A*, vol. 93, no. 3, Mar. 2016, Art. no. 033809.
- [19] P.-Y. Chen et al., "Generalized parity-time symmetry condition for enhanced sensor telemetry," *Nature Electron.*, vol. 1, no. 5, pp. 297–304, May 2018.
- [20] H. Kazemi, M. Y. Nada, F. Maddaleno, and F. Capolino, "Experimental demonstration of exceptional points of degeneracy in linear time periodic systems and exceptional sensitivity," 2019, arXiv:1908.08516.
- [21] H. Kazemi et al., "Ultra-sensitive radio frequency biosensor at an exceptional point of degeneracy induced by time modulation," 2019, arXiv:1909.03344.
- [22] E. S. Cassedy and A. A. Oliner, "Dispersion relations in time-space periodic media: Part I–stable interactions," *Proc. IEEE*, vol. 51, no. 10, pp. 1342–1359, Oct. 1963.

- [23] E. S. Cassedy, "Dispersion relations in time-space periodic media part II—Unstable interactions," *Proc. IEEE*, vol. 55, no. 7, pp. 1154–1168, Jul. 1967.
- [24] C. Elachi, "Electromagnetic wave propagation and wave-vector diagram in space–time periodic media," *IEEE Trans. Antennas Propag.*, vol. AP-20, no. 4, pp. 534–536, Jul. 1972.
- [25] J. R. Zurita-Sanchez, P. Halevi, and J. C. Cervantes-Gonzalez, "Reflection and transmission of a wave incident on a slab with a time-periodic dielectric function  $\epsilon(t)$ ," *Phys. Rev. A*, vol. 79, no. 5, May 2009, Art. no. 053821.
- [26] J. S. Martínez-Romero, O. M. Becerra-Fuentes, and P. Halevi, "Temporal photonic crystals with modulations of both permittivity and permeability," *Phys. Rev. A*, vol. 93, no. 6, Jun. 2016, Art. no. 063813.
- [27] N. A. Estep, D. L. Sounas, and A. Alu, "Magnetless microwave circulators based on spatiotemporally modulated rings of coupled resonators," *IEEE Trans. Microw. Theory Techn.*, vol. 64, no. 2, pp. 502–518, Feb. 2016.
- [28] S. Taravati and C. Caloz, "Mixer-duplexer-antenna leaky-wave system based on periodic space-time modulation," *IEEE Trans. Antennas Propag.*, vol. 65, no. 2, pp. 442–452, Feb. 2017.
- [29] H. Rajabalipanah, A. Abdolali, and K. Rouhi, "Reprogrammable spatiotemporally modulated graphene-based functional metasurfaces," *IEEE J. Emerg. Sel. Topics Circuits Syst.*, vol. 10, no. 1, pp. 75–87, Mar. 2020.
- [30] S. Qin, Q. Xu, and Y. E. Wang, "Nonreciprocal components with distributedly modulated capacitors," *IEEE Trans. Microw. Theory Techn.*, vol. 62, no. 10, pp. 2260–2272, Oct. 2014.
- [31] K. A. Lurie and V. V. Yakovlev, "Energy accumulation in waves propagating in space- and time-varying transmission lines," *IEEE Antennas Wireless Propag. Lett.*, vol. 15, pp. 1681–1684, 2016.
- [32] F. Wu, Y. Zheng, F. Yuan, and Y. Fu, "Magnetic-free isolators based on time-varying transmission lines," *Electronics*, vol. 8, no. 6, Jun. 2019, Art. no. 684
- [33] X. Wu, X. Liu, M. D. Hickle, D. Peroulis, J. S. Gomez-Diaz, and A. A. Melcon, "Isolating bandpass filters using time-modulated resonators," IEEE Trans. Microw. Theory Techn., vol. 67, no. 6, pp. 2331–2345, Jun. 2019.
- [34] M. A. K. Othman, M. Veysi, A. Figotin, and F. Capolino, "Low starting electron beam current in degenerate band edge oscillators," *IEEE Trans. Plasma Sci.*, vol. 44, no. 6, pp. 918–929, Jun. 2016.
- [35] Z. Yu and S. Fan, "Complete optical isolation created by indirect interband photonic transitions," *Nature Photon.*, vol. 3, no. 2, pp. 91–94, Feb. 2009.
- [36] A. Figotin and I. Vitebskiy, "Slow-wave resonance in periodic stacks of anisotropic layers," *Phys. Rev. A*, vol. 76, no. 5, Nov. 2007, Art. no. 053839.
- [37] J. Moro, J. V. Burke, and M. L. Overton, "On the Lidskii–Vishik– Lyusternik perturbation theory for eigenvalues of matrices with arbitrary Jordan structure," SIAM J. Matrix Anal. Appl., vol. 18, no. 4, pp. 793–817, Oct. 1997.
- [38] A. Welters, "On explicit recursive formulas in the spectral perturbation analysis of a Jordan block," *SIAM J. Matrix Anal. Appl.*, vol. 32, no. 1, pp. 1–22, Jan. 2011.
- [39] G. W. Hanson, A. B. Yakovlev, M. A. Othman, and F. Capolino, "Exceptional points of degeneracy and branch points for coupled transmission lines—Linear-algebra and bifurcation theory perspectives," *IEEE Trans. Antennas Propag.*, vol. 67, no. 2, pp. 1025–1034, Feb. 2019.
- [40] W. Chen, S. Kaya Ozdemir, G. Zhao, J. Wiersig, and L. Yang, "Exceptional points enhance sensing in an optical microcavity," *Nature*, vol. 548, no. 7666, pp. 192–196, Aug. 2017.
- [41] H. Hodaei et al., "Enhanced sensitivity at higher-order exceptional points," *Nature*, vol. 548, no. 7666, pp. 187–191, Aug. 2017.
- [42] F. Ellinger, H. Jackel, and W. Bachtold, "Varactor-loaded transmission-line phase shifter at C-band using lumped elements," *IEEE Trans. Microw. Theory Techn.*, vol. 51, no. 4, pp. 1135–1140, Apr. 2003.
- [43] K. Rouhi, H. Rajabalipanah, and A. Abdolali, "Multi-bit graphene-based bias-encoded metasurfaces for real-time terahertz wavefront shaping: From controllable orbital angular momentum generation toward arbitrary beam tailoring," *Carbon*, vol. 149, pp. 125–138, Aug. 2019.
- [44] A. Komar et al., "Dynamic beam switching by liquid crystal tunable dielectric metasurfaces," ACS Photon., vol. 5, no. 5, pp. 1742–1748, Feb. 2018.